J. Power Sources 2011; 196 (9): 4404-4410

Biogas reforming on La-promoted NiMgAl catalysts derived from hydrotalcite-like precursors

A. Serrano-Lotina[1]*, L. Rodríguez[1], G. Muñoz[1], L. Daza[1,2]

[1] Instituto de Catálisis y Petroleoquímica (CSIC), C/ Marie Curie 2, Campus Cantoblanco, 28049 Madrid, Spain.
[2] Ciemat, Av. Complutense 22, 28040 Madrid, Spain

* To whom the correspondence should be addressed: Instituto de Catálisis y Petroleoquímica. C/ Marie Curie 2. Campus de Cantoblanco. 28049 Madrid, Spain. phone: +34 91 5854793. Fax: +34 91 5854760. E-mail: asl@icp.csic.es

Abstract

Hydrotalcite-like precursors have been synthesized in order to study the influence of lanthanum on the structure and the properties of the precursors, as well as on the catalytic activity and stability of their derived catalyst on biogas reforming. From XRD, and TPO characterization, we confirmed that hydrotalcite-like precursors where obtained. After calcination at 750 ºC, Mg (Ni,Al)O solid solution was detected. High surface areas have been obtained finding the highest surface area on the catalyst without lanthanum. TPR experiments were performed in order to study the reducibility of the catalysts. One reduction peak was found in the catalyst without lanthanum while two peaks were observed in the catalysts with lanthanum. A reduction peak at 900 ºC was observed over the sample without Ni and La. Catalytic tests, at 700 ºC with a feed of CH_4:CO_2 1:1, were performed after appropriate reduction during 50h. While a decrease on catalytic activity was observed with the addition and the increase of La content, an enhancement in the stability was observed. No sign of deactivation of the catalyst and no carbon deposition were found on the catalysts doped with lanthanum.

Keywords: Biogas, reforming, hydrogen, hydrotalcite, Lanthanum.

1. Introduction

As a consequence of the effect of Global Warming in Climate Change, many efforts are being made in order to reduce Greenhouse gases and to produce clean energy. Renewable energy, as hydrogen production from renewable sources, is growing significantly in importance. Green hydrogen can be obtained from biogas (mainly, a mixture of CH_4 and CO_2) which is produced by the anaerobic digestion of organic matter present on waste. Since both methane and carbon dioxide are greenhouse effect gases, dry reforming of methane does not only provide renewable hydrogen but also reduces the emission of greenhouse gases because of the conversion of CH_4 and the indirect effect of avoided CO_2 emissions that result from conventional energy production [1]. In addition, CO_2 reforming of methane (1) avoids the separation of CO_2, which is an energy intensive and a rather costly process when steam reforming is used instead. Furthermore, contrary to steam reforming, in CO_2 reforming of methane it is not necessary to evaporate great quantities of water which it is also an energy demanding step [2].

$$CH_4 + CO_2 \leftrightarrows 2H_2 + 2CO \qquad \Delta H^o_{298} = + 247\ kJ \cdot mol^{-1} \quad (1)$$

The most important drawback of this reaction is deactivation, mainly produced by carbon formation, which is mainly produced by methane decomposition (2) and CO disproportionation (3) [3]:

$$CH_4 \leftrightarrows 2H_2 + C \qquad \Delta H^o_{298} = + 75\ kJ \cdot mol^{-1} \quad (2)$$

$$2CO \leftrightarrows CO_2 + C \qquad \Delta H^o_{298} = - 173\ kJ \cdot mol^{-1} \quad (3)$$

Noble metal catalysts are less sensitive to coking than Ni-based catalysts, probably due to the lower solubility of carbon in noble metals [3]. However, considering their high cost and limited availability, a deeper study on Ni-based catalyst is being carried out. Important variables to study in order to avoid coke formation are

the nature of the support [4-9] and the addition of promoters, as alkali metals or other promoters as V [10-12] which modify the Ni active phase inhibiting the activity and the deactivation by carbon formation. Lanthanides are suggested to be good promoters as they can strengthen CO_2 adsorption on support what hinders the formation of deposited carbon via reverse disproportionation [13]. Another theory about coke avoidance is reported by Verykios [14] who suggested that the oxycarbonate on the La_2O_3 support might be considered as a dynamic oxygen pool, which favours the removal of coke. They also retard metal sintering as a consequence of the high dispersion of the metal, which will improve coke resistance [15,16].

The preparation method is another important parameter as it can help coke avoidance. Wet impregnation synthesis is the most common preparation method. However, it produces some heterogeneity in the distribution of metal surface and a poor dispersion of metallic species which can favour coke formation. The use of precursors in which the metal is homogeneously distributed, may result, after calcination and reduction, in the formation of highly dispersed and stable metal particles on the surface [16]. Catalysts derived from hydrotalcite-like precursors have shown high dispersion and formation of small particles of the active metal what makes that Ni particles sinter less easily, as well as high surface area and basic properties which improved CO_2 chemisorption [17] and consequently the resistance to coke formation. Hydrotalcites are represented by the general formula:

$$[M(II)_{1-x}M(III)_x(OH)_2]^{x+} (A^{n-}_{x/n}) \cdot mH_2O$$

The structure of hydrotalcite is based on brucite structure, $Mg(OH)_2$, where octahedral of Mg^{2+} share edges to form sheets. Mg^{2+} is coordinated with OH^- ligands. The sheets are stacked on top of each other and held together by hydrogen bonding. When Mg^{2+} ions are substituted by a trivalent cation, as Al^{3+}, a positive charge is

generated which can be compensated by anions as CO_3^{2-}. These anions lie in the interlayer region between the two brucite-like sheets, where water of crystallization is also present [17].

Different preparation techniques have been reported for the synthesis of hydrotalcites, being co-precipitation method under low supersaturation condition the better option in order to obtain the most crystalline phase [17, 18] and to efficiently incorporate the transition metal [19]. In addition, the interlayered carbonate and the increase in the cristallinity of the structure seem to provide thermal stability to the samples [20]. Precipitation at low supersaturation is performed by slow addition of mixed solutions of divalent and trivalent metal salts with appropriate ratio into a reactor containing an aqueous solution of the desired interlayer anion. A second solution of an alkali is added into the reactor simultaneously at a fixed pH to promote co-precipitation of the metallic salts.

The use of hydrotalcites as catalyst precursors have been already studied on dry reforming of methane. Good activities have been reported [21-23], but operating at high reaction temperatures. In order to decrease reaction temperature, hydrotalcies have been doped with Ru and Ce, reaching better stabilities [24, 25]. The aim of this work is mainly to study the influence of La on reaction stability but also on catalytic activity and on catalytic properties.

2. Experimental

2.1. Precursors and catalysts preparation

Four precursors, denoted as sHT2, HT2, LaHT2 and 2LaHT2 where synthesized. Number 2 means that Mg/Al ratio is 2, sHT2 is a precursor that only contains Mg and Al, HT2 a precursor with 2% Ni (nominal weight), LaHT2 a precursor that contains 2%

Ni and 1% La (nominal weight) and 2LaHT2 a precursor that contains 2%Ni and 2%La (nominal weight).

HT precursors were prepared by co-precipitation at pH = 8 and at 60 ºC and continuous stirring by adding dropwise an aqueous solution containing $Mg(NO_3)_2 \cdot 6H_2O$ (Panreac, 98% assay), $Al(NO_3)_3 \cdot 9H_2O$ (Panreac, 98.0-102.0% assay), $Ni(NO_3)_2 \cdot 6H_2O$ (Panreac, 99% assay) and $La(NO_3)_2 \cdot 6H_2O$ (Panreac, 99,0% assay) to an aqueous solution containing $NaHCO_3$ (Panreac, 99.7-100.3% assay) at pH = 8, followed by ageing for 90 minutes at 60 ºC. pH was adjusted with a mixture of $NaHCO_3$ and NaOH solution (Riedel-de-Haën, 99% assay). Special care of filtering and precipitate washing was taken in order to eliminate Na^+ ions completely. Precursors were dried overnight at 110 ºC and calcined at 750 ºC for 2 h with a rate of 5 ºC·min^{-1} obtaining HT2-750 and LaHT2-750 catalysts and the reference sample sHT2-750. They were calcined at 750 ºC in order to assure their integrity on reaction, which is performed at 700 ºC.

2.2. Precursors and catalysts characterization

Composition of the precursors and their catalysts was determined after acid digestion by an ICP-MS Elan 6000 Perkin-Elmer Sciex equipped with an autosampler AS 91. Specific surface area of the catalyst was measured by the BET method using N_2 at -196 ºC with a Micromeritics ASAP 2010. X-ray diffraction of the precursors and their catalysts were performed on an X-ray diffractometer (XPERT- PRO, PANanalytical) using Cu Kα radiation (λ = 0.154 nm). Temperature programmed oxidation (TPO) of the precursors were performed in the temperature range of 25-950 ºC (5 ºC·min^{-1}) with a mixture of O_2/N_2 10/40 mLN·min^{-1} using a Mettler-Toledo TGA/SDTA 851 thermo-balance and STAR 8.10 software coupled to a mass spectrometer detector Pfeiffer Thermostar where m/z of 18 and 44 where followed in

order to characterized the desorptions. Temperature programmed reduction (TPR) of the catalysts were performed in the temperature range of 25-950 ºC (10 ºC·min^{-1}) feeding 50 mLN·min^{-1} of H_2, with the same equipment as TPO. Reduction was followed by water desorption on the mass spectrometer detector (m/z = 18) as hydrogen consumption cannot be detected.

2.3 Catalytic tests

Catalytic tests were carried out in Microactivity Reference PID Eng&Tech equipment. They were performed in tubular fixed-bed quartz reactor at 700 ºC and a CH_4:CO_2 molar ratio of 1:1 (biogas stream enriched with CO_2). It is remarkable that ratios of 1:1.2 are normally used in order to partially inhibit coke formation, because as the oxidant is in excess, CO_2 methane reforming reaction (2) is shift to hydrogen production, while disproportionation reaction (3) is shift to the gasification of C deposits leading to CO. Conversions lower than 40% were studied in order to evaluate the activity of the catalysts. For that purpose catalyst mass of 40 mg were employed with a mass/feed alimentation ratio (W/F) of 0.4 mg·min·cm^{-3}, at a reaction temperature of 700 ºC. The reaction products were analysed with an Agilent chromatograph 6890N connected in line, equipped with a TCD detector.

3. Results and discussion

3.1. Precursors characterization

Table 1 shows the chemical analysis of the precursors, performed by ICP-MS. While sHT2 molar ratio is the expected, HT2, LaHT2 and 2LaHT2 have ratios lower than the theoretical (Mg/Al ratio =2). This can be due to the substitution of Mg by Ni,

leading to lower Mg/Al ratios. If (Mg+Ni)/Al ratios are calculated, values nearer the theoretical are obtained, despite being lower yet. Ni and La contents were almost what were expected, being %Ni lower on 2LaHT2.

Fig. 1 shows the X-ray diffractograms of the precursors. They show the profile of the carbonated phase of hydrotalcite [17]. The intensity of the peak at 36º is higher than the intensity of the peak at 11º. This difference can be due to a disorder in the stacking of the layers, which also decreases the symmetry. No peak related to lanthanum species can be seen, what can be due to a low concentration or a high dispersion. A higher cristallinity of sHT2 is observed in comparison with the others precursor as narrower peaks are obtained. This result was also observed by Shishido *et. al.* [22].

Crystallographic parameters of hydrotalcites (Table 2) were calculated according to Casenave *et al.* [26], where $c = 3d_{0\ 0\ 3}$(spacing between layers) and $a = 2d_{1\ 1\ 0}$ (distance between cations), and compared with the results obtained by a hydrotalcite of Mg/Al ratio of 2 obtained by Cantrell *et al.* [27]. The spacing between layers in sHT2, HT2, LaHT2 and 2LaHT2 (Mg/Al molar ratios of 2.0, 1.8, 1.7 and 1.8, respectively) is slightly smaller than the one reported by Cantrell *et al.* [27], what could be due to a variable hydratation degree [28] or to a change in electrostatic attraction between the positive hydroxide layers and the negative interlayers [29]. No changes in the distance between cations were detected. If La was in the interlayer, *c* parameter would be higher on LaHT2 precursor and if it was inserted in the brucite-like layers *a* parameter would be higher due to its large ionic radious. Therefore, we can suppose that La is deposited over the surface, as other authors have proposed [24].

Regarding to TPO-MS of the precursors, three processes can be differentiated (Fig. 2) as other authors have previously reported [17, 30, 31]. Between 25 and 250 ºC a loss of physisorbed H_2O and CO_2 and interlaminar H_2O occurred, corresponding to a

weight loss of 14-16%. Dehydroxilation and loss of interlaminar CO_2 is observed between 250 and 600 ºC, representing a 22-26 % weight loss. At this temperature range, elimination of nitrates was also found. Finally, chemisorbed CO_2 in the most basic centres is lost at 700 ºC, corresponding to a weight loss of 3-4%. Velu *et al.* [32] attributed this peak to desorption of carbonate anions in the interlayer which form an oxiycarbonate with brucite sheets. It can be seen that this peak produced a weight loss slightly lower in sHT2. In addition, the profile of sHT2 is shifted to higher temperatures than in HT2 and LaHT2 what indicates that pure MgAl hydrotalcite is thermically more stable than hydrotalcites containing Ni and/or La.

This higher thermal stability may be a consequence of the higher cristallinity of the structure [20, 29], as XRD characterization showed (Fig. 1). Comparing HT2, LaHT2 and 2LaHT2, it can be seen that when La is added peak at 400 ºC acquires more importance that peak at 300 ºC, contrary to what is observed in HT2. When La content is increased, the peak at 300 ºC almost disappear. These facts may be due to the interaction between La and CO_2, what leads to a higher thermal stability.

3.2. Catalysts characterization

As calcination leads to H_2O and CO_2 loss, an increase in Ni and La relative content is expected with regard to their precursors. Ni content is 2.6, 2.9 and 2.9% in HT2-750, LaHT2-750 and 2LaHT2-750, respectively, while La content was 1.6% on LaHT2-750 and 3.1% on 2LaHT2-750.

Fig. 3 shows the XRD profile of sHT2-750, HT2-750, LaHT2-750 and 2LaHT2-750. It can be seen that after calcination, hydrotalcite structure is lost, leading to a mixture of oxides with diffraction bands at 37, 43, 63, 75 and 79º that may correspond to Mg(Ni,Al)O solid solution. No peak related to lanthanum can be seen, probably due

to its low concentration or its high dispersion. Again, a decrease in crystallinity with the increase of La content is detected.

The value of cell parameter *a* (Table 3) is in all cases smaller than that of pure MgO (4.21 Å), and also smaller than that calculated on the basis of Vegard's law, by linear interpolation of the pure oxides (4.21 Å). Both values are equivalent due to the higher proportion of MgO in comparison with NiO. This decrease in *a* parameter could be due to the presence of Al^{3+} ions in the Ni-Mg-O cubic lattice, having Al^{3+} an ionic radius smaller than Mg^{2+} and Ni^{2+}. This is also corroborated by diffraction absence of the possible crystalline phases of Al_2O_3.

BET areas of sHT2-750, HT2-750, LaHT2-750 and 2LaHT2-750 were also determined (Table 3). These high areas (82, 203, 157 and 107 $m^2 \cdot g^{-1}$, respectively), are attributed to the removal of H_2O and CO_2 during calcination (what was observed in TPO experiments), which leads to formation of channels and pores [33]. The lower BET area in sHT2-750 corroborates the higher thermal stability with the higher Mg content [34]. However, this value is much lower than others reported on literature [35]. The decrease of BET areas when La is added can be due to the location of La_2O_3 in the pores of the particles.

By TPR characterization (Fig. 4), a peak at 100 ºC was observed in all samples, which are consequence of the elimination of physisorbed H_2O and CO_2 already present on the catalysts. TPR profile of HT2-750 showed only one reduction peak at 800 ºC approximately. This high reduction temperature corresponds to reduction of thermal stable phase such as periclase Mg(Ni, Al)O, which present high reduction temperature due to electron transfer from NiO to MgO involving strong interactions between NiO and MgO and therefore a decrease in Ni reducibility [29, 36]. These results agree with what was reported by other authors [25, 37, 38]. This implies that the reduction of Ni at

700 ºC (our reaction temperature) is partial, remaining part of Ni as Ni^{2+} in Mg(Ni, Al)O. In LaHT2-750 another peak at 600 ºC is observed, what indicate that La promotes the reduction of Ni. As water desorption finishes at 650 ºC, this final temperature is chosen as the reduction temperature for the catalytic test of LaHT2-750. In 2LaHT2-750 two joined peaks are observed between 350 and 650 ºC, in addition to the 800 ºC peak. This also indicates the promotion of Ni reducibility by La, probably due to a better Ni dispersion. As water desorption also finishes at 650 ºC, this final temperature is chosen as the reduction temperature for the catalytic test of 2LaHT2-750.

None of the peaks described above were observed in sHT2-750 TPR experiment. However, H_2O desorption was observed at 900 ºC what can be due to the reduction of $MgAl_2O_3$.

BET areas were also measure after reduction treatment with 100 $mLN \cdot min^{-1}$ of H_2 at 700 ºC for HT2-750 and 650 ºC for LaHT2-750 and 2LaHT2-750 (Table 3). BET areas decrease but high BET areas are obtained yet. Therefore, no Ni sintering happened as a consequence of catalyst reduction.

3.3. Catalytic tests

In order to compare the activity of the catalysts (HT2-750, LaHT2-750 and 2LaHT2-750), they were tested in the conditions detailed in Experimental section. All tests were maintained in reaction for 50h in order to compare their stability. It can be noticed that CO_2 conversion in both catalysts are higher than CH_4 conversion (Fig.5). This can be explained by reverse water-gas-shift reaction (RWGS) (4), as it has been previously reported [15].

$$H_2 + CO_2 \leftrightarrows H_2O + CO \qquad (4)$$

Catalytic activity calculated by CH_4 conversion, is higher using HT2-750 catalyst (48.9 $molCH_4 \cdot h^{-1} \cdot g_{Ni}^{-1}$) than with LaHT2-750 (34.6 $molCH_4 \cdot h^{-1} \cdot g_{Ni}^{-1}$) and 2LaHT2-750 (21.9 $molCH_4 \cdot h^{-1} \cdot g_{Ni}^{-1}$). This may imply a better activity of the catalyst without La, contrary to what was observed by other authors as Daza *et al.*[39] and to the increase on Ni reducibility. An increase on La loading also decreases catalytic activity. We have to consider that reduction temperature is higher in HT2-750 catalyst, leading probably to a higher content of reduced Ni, so characterization of reducibility of catalysts should be made to study this fact.

While on reactions with LaHT2-750 and 2LaHT2-750 catalysts, no sign of desactivation was observed during the 50 h, in reaction with HT2-750, the conversion was decreasing from the beginning, with a rate of 0.09 $\%XCH_4 \cdot h^{-1}$.In the reaction with LaHT2-750 and 2LaHT2-750 catalyst, an initial induction period is observed what can be due to the interaction between CO_2 and La present on the catalyst [14]. Longer catalytic tests will be done on future in order to establish if 1% loading is enough to reach good stabilities.

Presence of H_2O in product distribution (Fig. 6) confirms that RWGS reaction is happening. It can be seen that it is similar in all the tests, despite the difference in CH_4 and CO_2 conversions. However, H_2 and CO do depend on conversions, being higher on HT2-750 due to the higher conversion. As the conversions are not total, CH_4 and CO_2 are also present on the output, being not represented here in order to simplify the graph.

Relation between CH_4 and CO_2 conversion and H_2/CO ratio (Fig. 7) are lower than what stochiometry indicates, as 1 mol of CH_4 and 1 mol of CO_2 react giving 2 moles of H_2 and 2 moles of CO, resulting in relations of XCH_4/XCO_2 and H_2/CO of 1. This is due to RWGS: CO_2 does not only react with CH_4 to produce H_2 and CO, but it also reacts with H_2 producing H_2O and CO. This makes that H_2/CO ratio decrease as H_2 is

consumed while CO is generated by this reaction. The differences on these relations found among tests are due to the differences in conversions.

It is noteworthy that a better stability on the catalysts with La has been obtained, as other authors have previously reported [14]. This could be consequence of $La_2O_2CO_3$ formation which gasificates coke deposits as well as a better dispersion of Ni favoured by La.

Temperature programmed oxidation (TPO) of catalysts after reaction was carried on in order to characterise coke deposits on catalyst surface (Fig. 8). On HT2-750 TPO experiment, a weight loss of 11% was detected, consequence of CO_2 formed by oxidation of coke. Coke formation rate can be calculated dividing the weight loss by the duration of the test. Coke formation rate of HT2-750 was 0.02 $mg_C \cdot mg_{cat}^{-1} \cdot h^{-1}$. Deposits of coke can be classified as Cγ or graphitic, according to its degasification temperature (600 ºC) [14]. A slight asymmetry of the peak suggests nickel carbide formation, which gasificate at 500 ºC [39]. A minor desorption was observed at 950 ºC with a weight loss of 0.2%. This C can be classified as inactive coke [40], which is very difficult to gasificate and therefore it is more prone to deactivate the catalyst as it can accumulate over the active phase.

On TPO experiment of LaHT2-750 and 2LaHT2-750 reduced at 650 ºC, coke deposits were not detected what confirms the great stability that was achieved during the 50 h reaction.

Post-reaction catalysts as well as fresh catalysts were also characterized by SEM (Fig. 9). Carbon filaments can be observed on Fig. 9b what confirm what was detected by TPO post-reaction characterization. As TPO post-reaction characterization showed, no coke was detected over LaHT2-750 and 2LaHT2-750 catalyst (Fig. 9d and 9f). Bright particles were found on LaHT2-750 and 2LaHT2-750 catalysts identified as

La_2O_3 from EDAX analysis. The higher stability observed on LaHT2-750 and 2LaHT2-750 could be explained by the interaction between Ni and La, which decorate catalyst surface producing higher Ni dispersion. This hypothesis should be evaluated by chemisorption experiments, in order to analyze Ni dispersion.

With regard of fresh HT2-750, LaHT2-750 and 2LaHT2-750 no significant differences were observed what can indicate that the different catalytic behaviour between catalysts is due to transformation of the catalysts when they are in contact with reaction feeding. La_2O_3 particles were found neither on the fresh nor on the reduced catalyst.

4. Conclusions

Four hydrotalcite-like precursors were synthesized as XRD and TPO have confirmed. Ni and La addition provoke a decrease on cristallinity. After calcination at 750 ºC, hydrotalcite-like structure decomposes, leading to Mg (Ni,Al)O solid solution. No peak related with lanthanum species can be seen, probably due to its low concentration or its high dispersion. TPR characterization showed that temperatures higher than 800 ºC are necessary in order to reduce all nickel. A peak at 650 ºC was also observed on LaHT2-750 and 2LaHT2-750 catalyst, consequence of the reduction of nickel interacting with La. High BET areas were detected in both catalysts, even after reduction.

Catalytic tests were carried on during 50 h after appropriate reduction, detecting higher activity on catalyst without La. The increase on La loading also decreases catalytic activity. However, much better stability was observed on the catalysts with La. No coke formation was observed contrary to HT2-750, where graphitic carbon was found. This highlights the importance of reduction temperature.

ACKNOWLEDGEMENTS

Financial support from Comunidad de Madrid (DIVERCEL-CM, S2009/ENE-1475) and CDTI (CENIT 2007-1039) is gratefully acknowledged.

REFERENCES

[1] L. Lombardi, E. Carnevale, A. Corti, Energy 31 (2006) 3208

[2] N. Muradov, F. Smith, A. T-Raissi, Int. J. Hydrogen Energy 33 (2008) 2023

[3] J.R. Rostrup-Nielsen, Stud. Surf. Sci. Catal. 81 (1994) 25

[4] S. Wang, G. Q. M. Lu, Appl. Catal. B 16 (1998) 269

[5] L. Xiancai, W. Min, L. Zhihua, H. Fei, Appl. Catal. A 290 (2005) 81

[6] B.Q. Xu, J.M. Wei, H.Y. Wang, K.Q. Sun, Q.M. Zhu, Catal. Today 68 (2001) 217

[7] S. Wang, G.Q. Lu, Appl. Catal. A 169 (1998) 271

[8] E. Ruckenstein, Y.H. Hu, Appl Catal A 133 (1995) 149

[9] K. Tomishige, O. Yamazaki, Y. Chen, K. Yokoyama, X. Li, K. Fujimoto, Catal. Today 45 (1998) 35

[10] J. Juan-Juan, M.C. Román-Martínez, M.J. Illán-Gómez, Appl. Catal. A 301 (2006) 9

[11] F. Pompeo, N.N. Nichio, M.G. Gonzalez, M. Montes, Catal. Today 107-108 (2005) 856

[12] A. Valentini, N.L. Villarreal, L. F. Dias, P. N. Lisboa-Filho, W.H. Schreiner, E. R. Leite, E. Longo, Appl. Catal. A 255 (2003) 211

[13] J.Z. Luo, Z.L. Yu, C.F. Ng, C.T. Au, J. Catal. 194 (2000) 198

[14] X. E. Verykios, I. J. Hydrogen Energy 28 (2003) 1045

[15] M. Benito, S. García, P. Ferreira-Aparicio, L. García Serrano, L. Daza, J. Power Sources 169 (2007) 177

[16] A. F. Lucrédio, G. Jerkiewickz, E.M. Assaf, Appl. Catal. A 333 (2007) 90

[17] F. Cavani, F. Trifirò, A. Vaccari, Catal. Today 11 (1991) 173.

[18] F. Prinetto, G. Ghiotti, P. Graffin, D. Tichit, Microp. Mesop. Mater. 39 (2000) 229

[19] A. Tsyganok, A. Sayari, J. Solid State Chem. 179 (2006) 1830

[20] M. Jitianu, M. Balasoiu, M. Zaharescu, A. Jitianu, A. Ivanov, J. Sol-Gel Sc. Tech. 19 (2000) 453

[21] A. Bhattacharyya, V. W. Chang, D. J. Schumacher, App. Clay Sci. 13 (1998) 317

[22] T. Shishido, M. Sukenobu, H. Morioka, R. Furukawa, H. Shirahase, K. Takehira, Catal. Lett. 73 (2001) 1

[23] F. Basile, G. Fornasari, E. Poluzzi, A. Vaccari, App. Clay Sci. 13 (1998) 329

[24] A. I. Tsyganok, M. Inaba, T. Tsunoda, K. Uchida, K. Suzuki, K. Takehira, T. Hayakawa, App. Catal. A 292 (2005) 328

[25] C. E. Daza, J. Gallego, J. A. Moreno, F. Mondragón, S. Moreno, R. Molina, Catal. Today 133-135 (2008) 357

[26] S. Casenave, H. Martinez, C. Guimon, A. Auroux, V. hulea, A. Cordoneanu, E. Dumitriu, Therm. Acta 379 (2001) 85-93

[27] D.G. Cantrell, L.J. Gillie, A.F. Lee, K. Wilson, Appl. Catal. A 287 (2005) 183.

[28] T. Lopez, P. Bosch, E. Ramos, R. Gomez, O. Novaro, D. Acosta, F. Figueras, Langmuir 12 (1996) 189

[29] O. Clause, M.G. Coelho, M. Gazzano, D. matteuzi, T. Trifirò, A. Vaccari, App. Clay Sci. 8 (1993) 169

[30] V. Rives, Mater. Chem. Phys. 75 (2002) 19

[31] V. Rives, S. Kannan, J. Mater. Chem., 10 (2000) 489

[32] S. Velu, C. S. Swamy, J. Mater. Sci. Lett. 15 (1996) 1674

[33] E.C. Kruissink, L.J. van Reijden and J.R.H. Ross, J. Chem. Soc., Faraday Trans. 1, 77 (1981) 649

[34] D. Tichit, F. Medina, B. Coq, R. Dutrartre, App. Catal. A 159 (1997) 241

[35] M. Bolognini, F. Cavani, D. Scagliarini, C. Flego, C. Perego, M. Saba, Micro. Meso. Mat. 66 (2003) 77

[36] A. F. Lucrédio, G. Jerkiewickz, E. M. Assaf, App. Catal. A 333 (2007) 90

[37] K. Takehira, T. Shishido, P. Wang, T. Kosaka, K. Takaki, J. Catal 221 (2004) 39

[38] A. Djaidja, S. Libs, A. Kiennemann, A. Barama, Catal. Today 113 (2006) 194.

[39] C.E. Daza, C.R. Cabrera, S. Moreno, R. Molina, Appl. Catal. A 378 (2010) 125

[40] J.J. Guo, H. Lou and X.M. Zheng, Carbon 45 (2007) 1314

TABLE CAPTIONS

Table 1: Chemical analysis of sHT2, HT2, LaHT2 and 2LaHT2 determined by ICP-MS.

	Mg/Al molar ratio		%Ni		(Mg+ Ni)/Al molar ratio	%La	
	Nominal	Experimental	Nominal	Experimental	Experimental	Nominal	Experimental
sHT2	2	2.0	---	---	2.0	---	---
HT2	2	1.8	2.0	1.9	1.9	---	---
LaHT2	2	1.7	2.0	2.1	1.8	1.0	1.1
2LaHT2	2	1.8	2.0	1.7	1.9	2.0	2.0

Table 2: Crystallographic parameters of sHT2, HT2, LaHT2 and 2LaHT2.

Precursor	Mg/Al molar ratio	c (Å)	a (Å)
sHT2	2.0	22.69	3.04
HT2	1.8	22.64	3.04
LaHT2	1.7	22.66	3.04
2LaHT2	1.7	22.46	3.03
Mg3 ([27])	1.8	23.25	3.04

Table 3: Crystallographic parameters and BET areas of sHT2-750, HT2-750, LaHT2-750 and 2LaHT2-750.

Catalyst	a (Å)	BET area ($m^2 \cdot g^{-1}$)	BET area ($m^2 \cdot g^{-1}$) after reduction
sHT2-750	4.19	82	---
HT2-750	4.19	203	162
LaHT2-750	4.18	166	142
2LaHT2-750	4.19	107	85

FIGURE CAPTIONS

Fig. 1: XRD patterns of sHT2, HT2, LaHT2 and 2LaHT2.

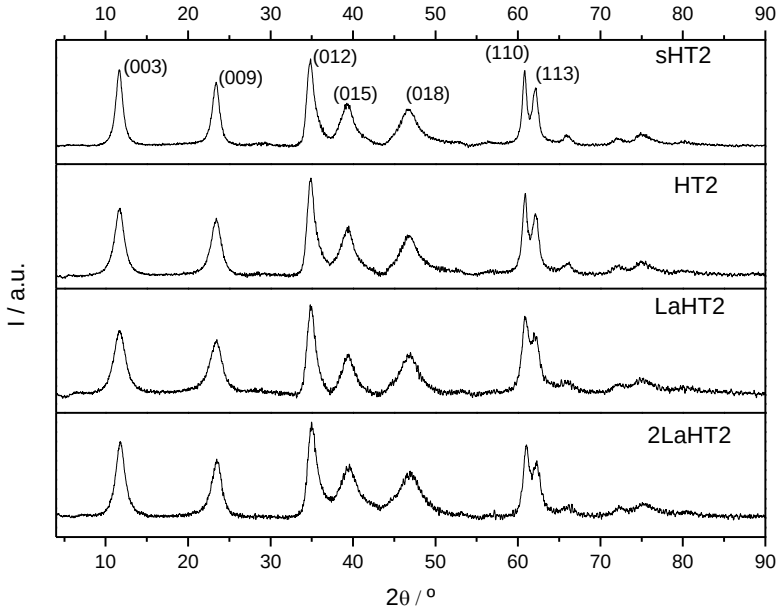

Fig. 2: TPO of sHT2, HT2, LaHT2 and 2LaHT2.

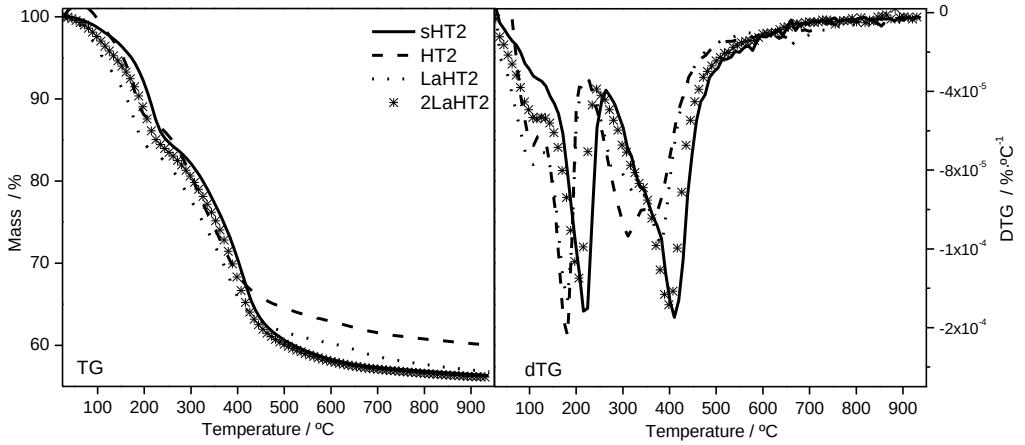

Fig. 3: XRD patterns of sHT2-750, HT2-750, LaHT2-750 and 2LaHT2-750.

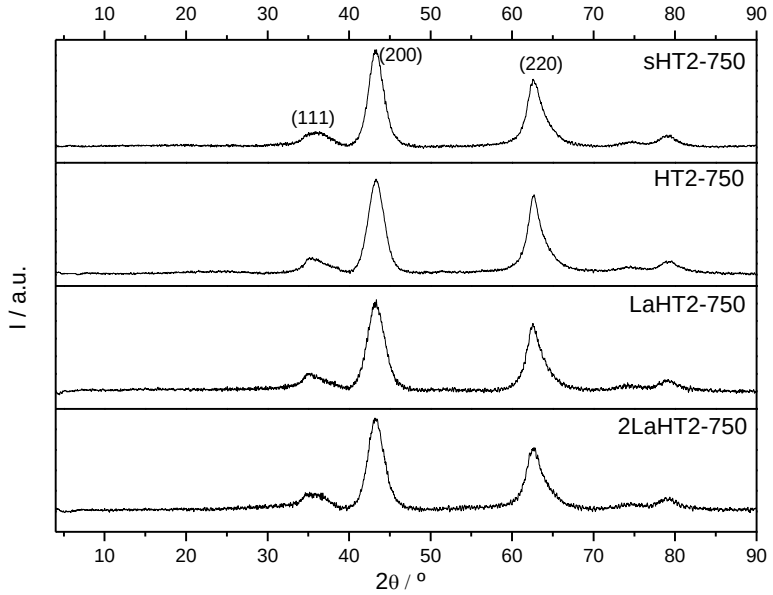

Fig. 4: TPR-MS of sHT2-750, HT2-750, LaHT2-750 and 2LaHT2-750.

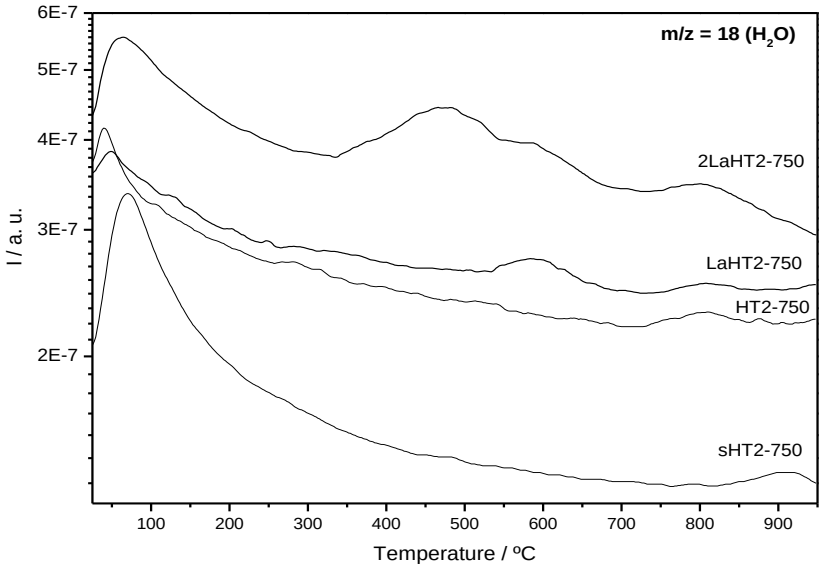

Fig. 5: CH_4 and CO_2 conversion *vs.* time in catalytic tests using HT2-750, LaHT2-750 and 2LaHT2-750 catalysts.

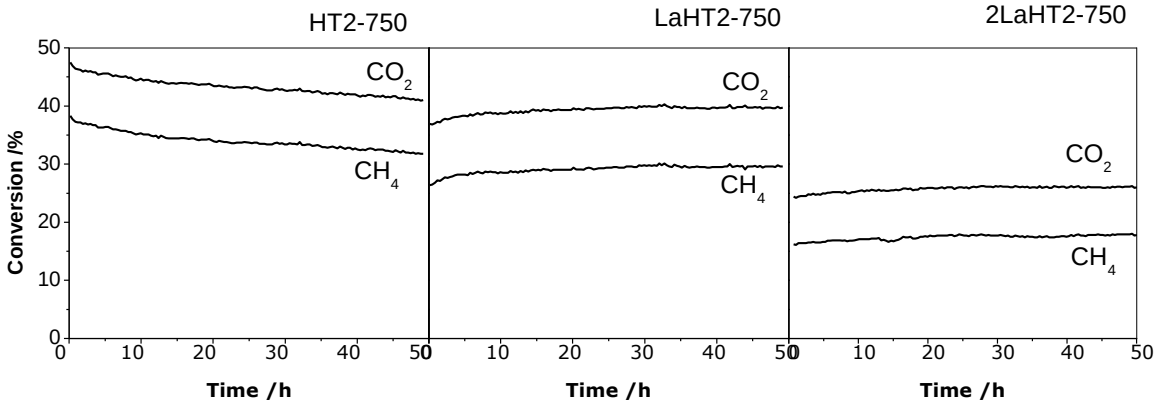

Fig. 6: Product distribution *vs.* time in catalytic tests using HT2-750, LaHT2-750 and 2LaHT2-750 catalysts.

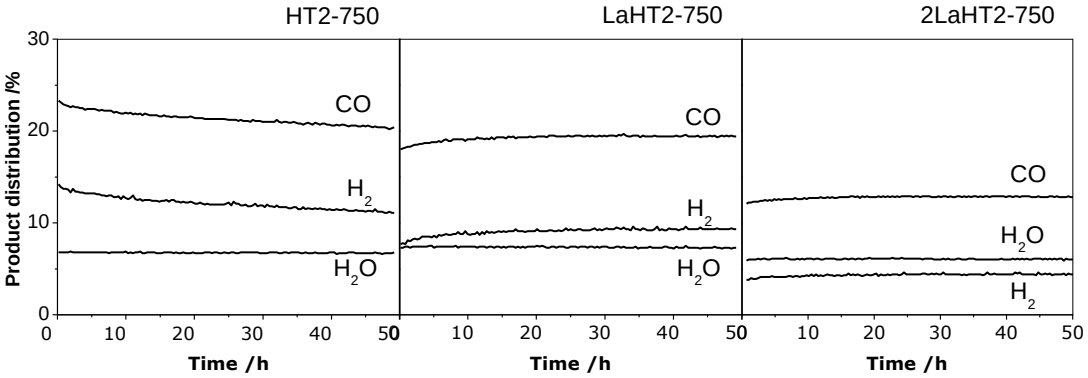

Fig. 7: XCH_4/XCO_2 and H_2/CO relations *vs.* time in catalytic tests using HT2-750, LaHT2-750 and 2LaHT2-750 catalysts.

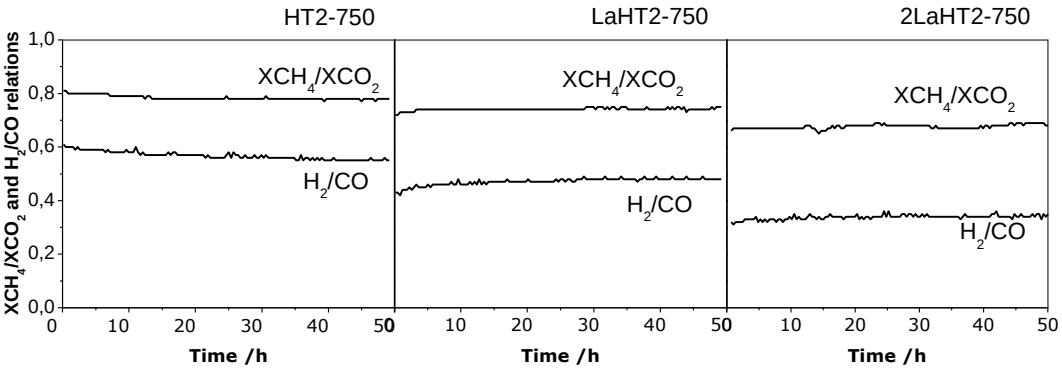

Fig. 8: TPO post-reaction of HT2-750, LaHT2-750 and 2LaHT2-750 catalysts.

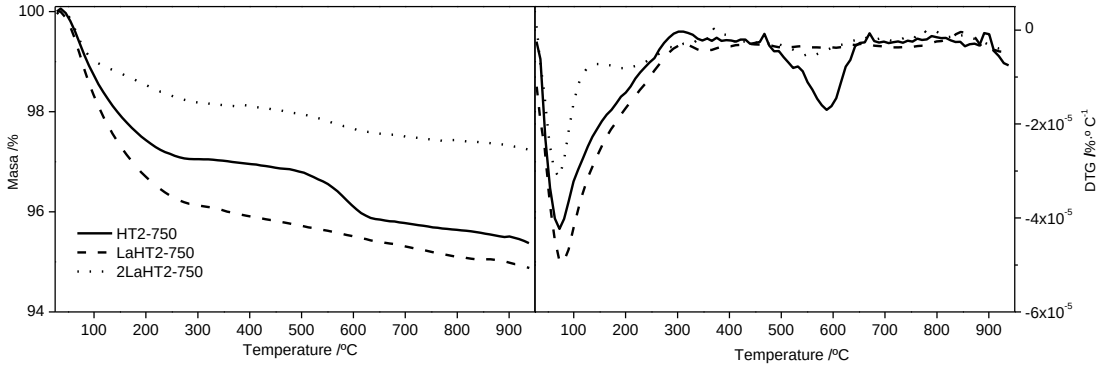

Fig. 9: SEM characterization of fresh and post-reaction HT2-750, LaHT2-750 and 2LaHT2-750 catalysts: (a) fresh HT2-750, (b) post-reaction HT2-750, (c) fresh LaHT2-750, (d) post-reaction LaHT2-750, (e) fresh 2LaHT2-750 and (f) post-reaction 2LaHT2-750.